NINETEENTH EUROPEAN ROTORCRAFT FORUM

Paper n° C10

NUMERICAL SIMULATION OF STEADY AND UNSTEADY EULER FLOWS AROUND MULTIBLADED HELICOPTER ROTORS

by

J.C. BONIFACE and J. SIDES

ONERA, B.P. 72, 92322 CHATILLON CEDEX, FRANCE

September 14-16, 1993
CERNOBBIO (Como)
ITALY

ASSOCIAZIONE INDUSTRIE AEROSPAZIALI

ASSOCIAZIONE ITALIANA DI AERONAUTICA ED ASTRONAUTICA

NUMERICAL SIMULATION OF STEADY AND UNSTEADY EULER FLOWS AROUND MULTIBLADED HELICOPTER ROTORS

by

J.C. BONIFACE and J. SIDES

ONERA, B.P. 72, 92322 CHATILLON CEDEX, FRANCE

Abstract

A space-centered implicit finite-volume Euler method is described and applied to the simulation of steady flow around multibladed helicopter rotors in hovering-flight in the framework of a pure capture of the wake. The method is then adapted to the computation of unsteady flows and applied to the simulation of the flow around an isolated blade submitted to an arbitrary solid body motion. A multibladed forward-flight flow simulation is achieved by the introduction of a wake correction.

1. - INTRODUCTION

Following pioneering works in U.S.A [1-10], and more recently in Europe [11,15], ONERA is developing, with the support of French Ministry of Defense (DRET), a research program for the introduction of Euler CFD tools in helicopter rotor flow simulation. Solving the Euler equations was identified as an important step for a numerical approach of the hovering-flight problem due to the possibility of theoretically taking into account the representation of the vortical wake system without particular treatment. This feature of the Euler equations is of great interest due to the importance of the mutual influence of the blades on the performance of a hovering rotor.

In a previous work [16], the application of a new implicit space-centered Euler solver without artificial viscosity due to Lerat, was described and illustrated for the simulation of the steady flow around the classical two-bladed model rotor of US-Army in hovering-flight in the framework of a calculation with pure capture of the wake. This new contribution is devoted to present the improvements carried on the steady hover method and to develop its extension for the calculation of unsteady transonic flows around rotors in forward-flight.

In a first chapter, the different formulations of the Euler equations in a rotating frame, used for the various steady and unsteady applications considered, are described in details. In a second chapter, the numerical method is presented with emphasis on its finite-volume formulation deduced from a direct approximation of the Euler equations in integral conservation-law form. The last chapter is devoted to the description of the applications.

2. - GOVERNING EQUATIONS

2.1 - General formulation of the Euler equations in integral conservation-law form

We consider the problem of an inviscid flow over a helicopter rotor in forward flight with a velocity $\vec{V}_0$. The blades are rotating with velocity $\vec{\Omega}$ and are submitted to pitching and flapping motions with respect to an absolute cartesian frame R_a $(0, \vec{x}, \vec{y}, \vec{z})$. In the absolute frame R_a, the flow is governed by the system of three-dimensional compressible unsteady Euler equations written below in integral conservation-law form applied on a computational domain $\Omega(t)$ with moving boundary $\Gamma(t)$ of outward normal $\vec{n}(t)$ and driven velocity $\vec{s}(t)$:

$$(1a)\quad \frac{d}{dt}\int_{\Omega(t)} \rho\, d\Omega + \int_{\Gamma(t)} [\vec{V} - \vec{s}(t)] \cdot \vec{n}(t)\, \rho\, d\Gamma = 0\ ,$$

$$(1b)\quad \frac{d}{dt}\int_{\Omega(t)} \rho\vec{V}\, d\Omega + \int_{\Gamma(t)} \left[[\vec{V} - \vec{s}(t)] \cdot \vec{n}(t)\, \rho\vec{V} + p\, \vec{n}(t)\right] d\Gamma = \vec{0}\ ,$$

$$(1c)\quad \frac{d}{dt}\int_{\Omega(t)} \rho E\, d\Omega + \int_{\Gamma(t)} \left[[\vec{V} - \vec{s}(t)] \cdot \vec{n}(t)\, \rho E + p\, \vec{V}.\vec{n}(t)\right] d\Gamma = 0\ .$$

In this system, the conservative unknowns, depending of the instantaneous spacial position $\vec{r}(t)$ of the points M of $\Omega(t)$, are : the density ρ, the momentum $\rho\vec{V}$, where $\vec{V}$ is the absolute flow velocity, and the energy E.

The pressure p is deduced from the thermodynamic law state : $p = (\gamma-1)\rho e$, where e is the specific internal energy defined by $e = E - |\vec{V}|^2/2$.

For the unsteady forward-flight application, it is suitable to use a "fully absolute" formulation of the system (1). More precisely, the momentum equations are formulated in the absolute frame R_a, and, in system (1), d/dt expresses the time derivative with respect to this absolute frame. We define [u, v, w] as the scalar components of the absolute velocity $\vec{V}$ projected in the absolute frame and we introduce the five-components vector of conservative unknowns :

$$(2)\quad W = [\rho, \rho u, \rho v, \rho w, \rho E]^T.$$

Then the system (1) can be written in the following condensed form :

$$(3a)\quad \frac{d}{dt}\int_{\Omega(t)} W\, d\Omega + \int_{\Gamma(t)} H[W, \vec{s}(t), \vec{n}(t)]\, d\Gamma = 0\ ,$$

$$(3b)\quad H[W, \vec{s}(t), \vec{n}(t)] = [\vec{V} - \vec{s}(t)] \cdot \vec{n}(t)\, W + p \begin{bmatrix} 0 \\ \vec{n}(t) \\ \vec{V} \cdot \vec{n}(t) \end{bmatrix}.$$

This general formulation has to be completed by *initial data and boundary conditions*. By example on a solid body surface the slip condition is :

$$(4)\quad \vec{V} \cdot \vec{n}(t) = \vec{s}(t) \cdot \vec{n}(t),$$

and on the body surface, the Euler flux depends only on the pressure, on the driven velocity $\vec{s}(t)$ of the boundary and on the metric $\vec{n}(t)$:

$$(5)\quad H[\, p, \vec{s}(t), \vec{n}(t)] = p \begin{bmatrix} 0 \\ \vec{n}(t) \\ \vec{s}(t) \cdot \vec{n}(t) \end{bmatrix}$$

2.2 - Formulation for an isolated rotor blade in forward flight with cyclic pitching and flapping motions

2.2.1 - Description of the motions (figure 1)

We consider an isolated helicopter blade in rotating, pitching and flapping motions with respect to the absolute frame $R_a = (O, \vec{x}, \vec{y}, \vec{z})$; the uniform translating advancing velocity motion $\vec{V}_0$ is taken into account *in the far-field boundary conditions.*

We define the relative frame $R_r(O, \vec{e}_1, \vec{e}_2, \vec{z})$ driven by an uniform rotating velocity $\vec{\Omega} = \omega\vec{z}$ around axis $O\vec{z}$ with respect to the absolute frame R_a (see figure 1a). The instantaneous angle $\psi_m(t)$ between the axis $\vec{Ox}$ and $\vec{Oe}_1$ is connected to the azimuthal angle $\psi(t)$ by the relation :

$$(6)\quad \psi_m(t) = \psi(t) - \pi/2, \quad \text{with } \psi(t) = \omega t.$$

In addition, the blade is in flapping motion around axis $O\vec{e}_1$ with angle $\beta(t)$ which defines the relative frame $R_f(O, \vec{e}_1, \vec{a}_2, \vec{a}_3)$ (see figure 1b) with the law:

(7) $\beta(t) = \beta_0 + \beta_{1c}\cos\psi(t) + \beta_{1s}\sin\psi(t)$, where β_0 is the conicity angle of the rotor.

Finally, the solid body motion is completed by cyclic pitching around axis $O\vec{a}_2$, with angle $\theta(t)$ defining the relative frame $R_p(O, \vec{x}_1, \vec{a}_2, \vec{z}_1)$ (see figure 1c). The instantaneous pitching angle is :

(8) $\theta(t) = \theta_0 + \theta_{1c}\cos\psi(t) + \theta_{1s}\sin\psi(t)$, where θ_0 is the collective pitch of the blade.

The rotating velocity of relative frame R_p with respect to the absolute frame R_a is then:

(9) $\vec{\Omega}(R_p/R_a) = \dot{\psi}_m(t)\,\vec{z} + \dot{\beta}(t)\,\vec{e}_1 + \dot{\theta}(t)\,\vec{a}_2$,

where the dot expresses the time-derivative and we have :

(10) $$\vec{\Omega}(R_p/R_a) = \begin{bmatrix} \dot{\beta}\cos\theta(t) - \omega\cos\beta(t)\sin\theta(t) \\ \dot{\theta}(t) + \omega\sin\beta(t) \\ \dot{\beta}\sin\theta(t) + \omega\cos\beta(t)\cos\theta(t) \end{bmatrix}$$ in the relative frame R_p.

We introduce the transformation matrix S(t), between the two frames R_a and R_p, which is a product of the three rotation matrices of angles $\psi_m(t)$, $\beta(t)$, $\theta(t)$:

(11) $$S(t) = \begin{bmatrix} \cos\theta\cos\psi_m - \sin\theta\sin\beta\sin\psi_m & -\cos\beta\sin\psi_m & \sin\theta\cos\psi_m + \cos\theta\sin\beta\sin\psi_m \\ \cos\theta\sin\psi_m + \sin\theta\sin\beta\cos\psi_m & \cos\beta\cos\psi_m & \sin\theta\sin\psi_m - \cos\theta\sin\beta\cos\psi_m \\ -\sin\theta\cos\beta & \sin\beta & \cos\theta\cos\beta \end{bmatrix}.$$

2.2.2 - Formulation in the case of a mesh-grid attached to the blade

The formulation developed below was first introduced in [17] for the solution of the two-dimensional unsteady Euler equations and application to transonic flow calculations around oscillating airfoils.

We define a mesh-grid Ω attached to the blade which does not vary in time in the relative frame R_p and the conservative variables of system (1) are now expressed with the coordinates $[x', y', z']$ of the relative frame R_p leading to an Eulerian description of the flow in this frame. In addition, in order to simplify the formulation, the scalar products are evaluated in the relative frame R_p. Each point M of the attached grid is fixed in the relative frame R_p and its driven velocity with respect to the absolute frame R_a is given by :

(12) $$\vec{s}(t) = \vec{V}(M/R_a) = \frac{d}{dt}\vec{r}(t)\Big|_{R_a} = \frac{d}{dt}\vec{r}(t)\Big|_{R_p} + \vec{\Omega}(R_p/R_a) \times \vec{r}(t) = \vec{\Omega}(R_p/R_a) \times \vec{r}(t)$$

We need to use the components of the vectors of the problem both in the absolute frame R_a and in the relative frame R_p. For notation commodity, and specially to allow later an easier description of the formulation used for the hovering-flight problem, we define :

(13) $\vec{r}(t) \equiv [x,y,z]^T|_{R_a} = S(t).[x',y',z']^T|_{R_a} = [x',y',z']^T|_{R_p} \equiv \vec{r}\,'$(not time-depending)

(14) $\vec{V} \equiv [u, v, w]^T|_{R_a} = S(t).[u', v', w']^T|_{R_a} = [u', v', w']^T|_{R_p} \equiv \vec{V}\,'$

(15) $\vec{n}(t) \equiv [n_x,n_y,n_z]^T|_{R_a} = S(t).[n'_x,n'_y,n'_z]^T|_{R_a} = [n'_x,n'_y,n'_z]^T|_{R_p} \equiv \vec{n}\,'$(not time-depending)

It is worth noticing that $\vec{V}$ and $\vec{V}'$ (resp. $\vec{r}$ and $\vec{r}\,'$, $\vec{n}$ and $\vec{n}\,'$) are two different representations of the same vector previously noted $\vec{V}$ (resp. $\vec{r}$, $\vec{n}$).

We introduce in a similar way :

(16a) $\vec{s}(t) = \vec{\Omega}(R_p/R_a) \times \vec{r}(t) \equiv \vec{\Omega}\,'(R_p/R_a) \times \vec{r}\,' \equiv \vec{s}\,'(t)$

with

(16b) $\vec{\Omega}\,'(R_p/R_a) \equiv \vec{\Omega}(R_p/R_a)\big|_{R_p}$ given by (10)

Using these notations, the conservation equations (1) can be rewritten as follows :

$$(17a)\quad \frac{d}{dt}\int_\Omega \rho\, d\Omega + \int_\Gamma [\vec{V}' - \vec{s}'(t)] \cdot \vec{n}'\, \rho\, d\Gamma = 0 ,$$

$$(17b)\quad \frac{d}{dt}\int_\Omega \rho\vec{V}\, d\Omega + \int_\Gamma \left[[\vec{V}' - \vec{s}'(t)] \cdot \vec{n}'\, \rho\vec{V} + p\, S(t)\, \vec{n}' \right] d\Gamma = \vec{0} ,$$

$$(17c)\quad \frac{d}{dt}\int_\Omega \rho E\, d\Omega + \int_\Gamma \left[[\vec{V}' - \vec{s}'(t)] \cdot \vec{n}'\, \rho E + p\, \vec{V}' . \vec{n}' \right] d\Gamma = 0 ,$$

or also in the condensed form :

$$(18a)\quad \frac{d}{dt}\int_\Omega W\, d\Omega + \int_\Gamma H[W, \vec{s}'(t), \vec{n}', t]\, d\Gamma = 0 ,$$

$$(18b)\quad H[W, \vec{s}'(t), \vec{n}', t] = [\vec{V}' - \vec{s}'(t)].\vec{n}'\, W + p \begin{bmatrix} 0 \\ S(t) \cdot \vec{n}' \\ \vec{V}' . \vec{n}' \end{bmatrix} .$$

It is worth pointing out that :

- the unknowns of the problem for the flow velocity, which are the components of the absolute velocity projected in the absolute frame, do not depend on the metric, that is suitable for an accurate treatment of the numerical finite-volume fluxes.
- the computational grid attached to the blade is fixed, and the unsteady fluxes depend explicitly, versus the time, only on the transformation matrix S(t) and the driven velocity $\vec{s}'$ expressed with (16a,16b), allowing an easy and economical coding,
- the unsteady formulation is formally identical, and so no more complicated, than the one used for a steady wing flow problem.

2.2.3 - Formulation in the particular case of an isolated rotor blade without cyclic pitching and flapping motions

For this problem the unsteady formulation (17-18) is slighter simplified. We have now $\beta(t) = \theta(t) = 0$ and all the relative frames R_r, R_f and R_p introduced in paragraph 2.2.1 are coinciding. Subsequently, we can introduce only the relative frame R_r attached to the blade in its rotating motion and we have from (9) or (10) :

$$(19)\quad \vec{\Omega}(R_r/R_a) = \omega\, \vec{z} = \vec{\Omega}'(R_r/R_a).$$

The driven velocity of the points of the boundary Γ does not depend on time when it is expressed in the relative frame R_r. Using (16),(13) and (19) we obtain :

$$(20)\quad \vec{s}' = \omega\, [-y', x', 0]^T,$$

and the transformation matrix S(t), between the absolute and relative frames, degenerates in the simple rotation matrix R(t) of axis $O\vec{z}$ and angle $\psi_m(t)$:

$$(21)\quad R(t) = \begin{bmatrix} \cos\psi_m(t) & -\sin\psi_m(t) & 0 \\ \sin\psi_m(t) & \cos\psi_m(t) & 0 \\ 0 & 0 & 1 \end{bmatrix}.$$

2.3 - Formulation for the multibladed rotor in hovering-flight

We consider the flow around a multibladed helicopter rotor in hovering-flight. In this problem the advancing velocity $\vec{V}_0$ is equal to zero and the rotor is submitted to an uniform rotating motion of velocity $\vec{\Omega}(R_r/R_a)$ given by expression (19). In the relative frame R_r attached to the rotor, the flow is steady and periodic with period $2\pi/N_b$ in the azimuthal direction, where N_b is the number of blades. The computational domain Ω, fixed in the

relative frame, can be restricted to a zone, around only one blade, covering a $2\pi/N_b$ part of the rotor; the influence of the other blades is taken into account exactly with the application of a periodicity boundary condition. The formulation developed previously for the simplified unsteady forward flight problem (2.23) could be used. However, in order to benefit of the steady character of the flow in the relative frame R_r, the momentum equations will be now formulated in this relative frame.

We introduce the time-derivative formula on a moving frame :

$$(22) \quad \frac{d}{dt} \int_\Omega \rho \vec{V} \, d\Omega = \frac{d}{dt'} \int_\Omega \rho \vec{V} \, d\Omega + \vec{\Omega}(R_r/R_a) \times \int_\Omega \rho \vec{V} \, d\Omega,$$

where d/dt' expresses the time-derivative with respect to the relative frame R_r. The time-derivative d/dt with respect to the absolute frame R_a can be eliminated by combining the expression (17b) with the driven velocity (20) and the formula (22) with the rotating velocity (19):

$$(23) \quad \frac{d}{dt'} \int_\Omega \rho \vec{V} \, d\Omega + \int_\Gamma \left[[\vec{V}' - \vec{s}'] \cdot \vec{n}' \, \rho \vec{V} + p \, R(t) \, \vec{n}' \right] d\Gamma = - \int_\Omega \vec{\Omega}(R_r/R_a) \times \rho \vec{V} \, d\Omega.$$

We first note the addition of a source term with respect to the previous formulation. Morever, the conservative fluxes still depend of the time. In order to simplify the formulation (without mixing of the scalar components of the absolute flow velocity projected in the absolute and relative frames), we will describe now the vectorial equation (23) in the relative frame R_r using the relations (14), (15) and (19):

$$(24) \quad \frac{d}{dt'} \int_\Omega \rho \vec{V}' \, d\Omega + \int_\Gamma \left[[\vec{V}' - \vec{s}'] \cdot \vec{n}' \, \rho \vec{V}' + p \, \vec{n}' \right] d\Gamma = - \int_\Omega \vec{\Omega}'(R_r/R_a) \times \rho \vec{V}' \, d\Omega \, ,$$

the formulation (17a,17c) for the mass and energy scalar equations being unmodified.

The unknowns of the problem for the flow velocity are now the scalar components of the absolute velocity projected in the relative frame and we define :

$$(25) \quad W' = [\rho, \rho u', \rho v', \rho w', \rho E]^T.$$

Finally, the complete formulation can be written using a compact form analogous to the one introduced previously (18) :

$$(26a) \quad \frac{d}{dt'} \int_\Omega W' \, d\Omega + \int_\Gamma H[W', \vec{s}', \vec{n}'] \, d\Gamma = \int_\Omega T(W') \, d\Omega,$$

$$(26b) \quad H[W', \vec{s}', \vec{n}'] = [\vec{V}' - \vec{s}'].\vec{n}' \, W' + p \begin{bmatrix} 0 \\ \vec{n}' \\ \vec{V}' . \vec{n}' \end{bmatrix} . ,$$

where the source term has the simple expression :

$$(27) \quad T(W') = \omega \, [0, \rho v', -\rho u', 0, 0]^T.$$

In this formulation the conservative fluxes do not depend explicity on the time and the source term only depends linearly on the conservative unknowns.

3. - NUMERICAL METHOD

3.1 - Finite-volume approximation

We consider the system of Euler equations on a general conservation-law form including all the particular cases studied in the previous chapter :

$$(28) \quad \frac{d}{dt} \int_\Omega W \, d\Omega + \int_\Gamma H[W, \vec{s}(t), \vec{n}, t] \, d\Gamma = \int_\Omega T(W) \, d\Omega \, ,$$

where W is the vector of conservative unknowns and H is the conservative Euler flux which can depend explictly on the time. We suppose that the source term T(W) depends only on the conservative unknowns. In addition the source term is supposed to be equal to zero in the case of the unsteady forward-flight formulation (18).

For a numerical approximation of system (28) on fixed domain Ω, we consider a curvilinear structured computational grid built of elementary cells $\Omega_{i,j,k}$, which volume and boundary are $V_{i,j,k}$ and $\Gamma_{i,j,k} = \bigcup_{I,J,K} \Gamma_{I,J,K}$, where $\Gamma_{I,J,K}$ represents any side of the cell $\Omega_{i,j,k}$.

The numerical method is in "conservation form", if it can be written as follows (see [18]) :

$$(29) \quad \frac{\Delta W_{i,j,k}}{\Delta t} + \frac{\sum_{I,J,K} H^{n+1/2}_{I,J,K}}{V_{i,j,k}} = T^{n+1/2}_{i,j,k},$$

with the introduction of the time-difference operator : $\Delta W = W^{n+1} - W^n$, where Δt is the time step and $W^n_{i,j,k}$ is an approximation of the mean value of W in the cell $\Omega_{i,j,k}$ at time $t^n = n\Delta t$:

$$(30) \quad \overline{W}^n_{i,j,k} = \frac{1}{V_{i,j,k}} \int_{\Omega_{i,j,k}} W \, d\Omega \, |_{t=t^n}.$$

The numerical flux $H^{n+1/2}_{I,J,K}$ is a consistent approximation of the mean value, during the time interval (t^n,t^{n+1}), of the conservative flux H across $\Gamma_{I,J,K}$:

$$(31) \quad \overline{H}^{n+1/2}_{I,J,K} = \frac{1}{\Delta t} \int_{t^n}^{t^{n+1}} \left[\int_{\Gamma_{I,J,K}} H[W, \vec{s}(t), \vec{n}, t] \, d\Gamma \right] dt,$$

and the term $T^{n+1/2}_{i,j,k}$ is an approximation of the mean value, during the time interval (t^n,t^{n+1}), of the contribution of the source terme in $\Omega_{i,j,k}$:

$$(32) \quad \overline{T}^{n+1/2}_{i,j,k} = \frac{1}{\Delta t} \int_{t^n}^{t^{n+1}} \left[\frac{1}{V_{i,j,k}} \int_{\Omega_{i,j,k}} T(W) \, d\Omega \right] dt.$$

The choice of a numerical scheme will allow to precize the approximation for the Euler flux and source term.

3.2 - Recall on the numerical method

In this work, the method used to solve the Euler equations for helicopter applications is based on a space-centered implicit solveur introduced by Lerat [18-20] and previously developed at ONERA, in the curvilinear finite-volume formulation, for the solution of steady transonic flows around airfoils [21,22]. We recall that this original space-centered solver works without artificial viscosity for steady transonic flow calculations. For application to the hovering-flight problem, the method is slightly modified due to the presence of a source term (see [20]). For the treatment of time-accurate problems the basic method is also slightly modified and very similar to the one previously developed for two-dimensional unsteady transonic applications [23-25].

3.3 - Description of the numerical method

3.3.1 - Explicit stage of the basic method for the rotor in hovering-flight

When system (28) is used for the description of the flow around a helicopter rotor in hovering-flight, we have previously shown that the conservative Euler flux depends only on time through the conservative unknowns (26), and also that the driven velocity does not depend on time (20). The boundary conditions being steady, the flow is also steady in the relative frame. So we have used the explicit stage of the basic method which corresponds to an original multidimensional extension of the Lax-Wendroff approximation, and can be easily

extended to the situation where the conservation equations contain an additional source term. This explicit stage introduces, because of the coupling between the Lax-Wendroff time-approximation and the original spacial discretization of the second order term, one predictor in each space direction and a corrector.

The expression of the explicit predictor $\Delta\tilde{W}_{I,J,K}$ will depend on each side $\Gamma_{I,J,K}$ of the grid-cell $\Omega_{i,j,k}$ and is calculated, using a discrete approximation of system (28), in a staggered cell $\Omega_{I,J,K}$ of boundary $\partial\Omega_{I,J,K}$ following the lines of the curvilinear grid :

$$(33) \quad \Delta\tilde{W}_{I,J,K} = -\frac{\Delta t}{2V_{I,J,K}} \left[\int_{\partial\Omega_{I,J,K}} H(W^n, \vec{s}, \vec{n})\, d\Gamma - \int_{\Omega_{I,J,K}} T(W^n)\, d\Omega \right].$$

A predictor calculation involves globally ten cells in the vicinity of the current cell $\Omega_{I,J,K}$ at time t^n (see figure 2).

Finally, an explicit numerical flux for the corrector is calculated accross each side of the current grid-cell from the value of the predictor and with the introduction of the jacobian matrix of the conservative flux :

$$(34) \quad A(W, \vec{s}, \vec{n}) = \frac{\partial H}{\partial W}\,(W, \vec{s}, \vec{n}).$$

The numerical flux expressed on the side $\Gamma_{I,J,K}$ is :

$$(35) \quad H^{n+1/2}_{I,J,K} = \int_{\Gamma_{I,J,K}} \left[H(W^n, \vec{s}, \vec{n}) + A(W^n, \vec{s}, \vec{n})\, \Delta\tilde{W} \right] d\Gamma$$

The fully discretization in space in the finite-volume formulation leads to a consistent approximation of (31).

Although expression (33) could be interpreted as a predictor step, the discretization introduced here comes from the second-order time-discretization of the Lax-Wendroff scheme and not from that of a kind of classical predictor-corrector scheme.

In the case of the approximation of a steady problem, where the consistency in time is not necessary, it is possible to simplify the time-discretization of the source term as it was done previously in [20]:

$$(36) \quad T^{n+1/2}_{i,j,k} = \frac{1}{V_{i,j,k}} \int_{\Omega_{i,j,k}} T(W^n)\, d\Omega.$$

The final explicit approximation is written under the conservation form (29) and give the explicit corrector :

$$(37) \quad \Delta W^{exp}_{i,j,k} = -\,\Delta t \left[\frac{\sum_{I,J,K} H^{n+1/2}_{I,J,K}}{V_{i,j,k}} - T^{n+1/2}_{i,j,k} \right],$$

leading to the use of globally twenty seven cells at time t^n.

The global contribution of the driven velocity to the numerical flux $\int_{\Gamma_{I,J,K}} W\,\vec{s}\,.\,\vec{n}\, d\Gamma$ can be calculated with accuracy due to its particular expression $\vec{s} = \omega\,\vec{z} \times \vec{r}$, in the case of the hovering-flight problem [11]. This calculation is described in [4] :

$$\int_{\Gamma_{I,J,K}} W\,\vec{s}\,.\,\vec{n}\, d\Gamma = \overline{W}_{I,J,K} \int_{\Gamma_{I,J,K}} \vec{s}\,.\,\vec{n}\, d\Gamma,$$

where $\overline{W}_{I,J,K}$ represents a mean value of W, on the side $\Gamma_{I,J,K}$, consistent with a finite-volume approximation, and which is calculated by using the current-cell scheme. The analytical calculation of the scalar product $\int_{\Gamma_{I,J,K}} \vec{s}\,.\,\vec{n}\, d\Gamma$, needs only the knownlegde of the vertices defining $\Gamma_{I,J,K}$. This calculation is done only one and stocked in the same way as the normal is.

3.3.2 - Explicit stage of the modified method for the blade in forward-flight

For the unsteady problem of the isolated blade submitted to an arbitrary rigid body motion, the numerical method is not fundamentally modified, due to the fact, in particular, that the system (28) does not contain any additional source term. However, the explicit time-dependency of the conservative flux (18), through the driven velocity and the transformation matrix between the two absolute and relative frames (11), introduces additional terms in the Lax-Wendroff time-discretization with jacobian matrices [26]. In order to simplify this discretization we have chosen to use a "S_β^α" explicit stage without matrices [18]. This explicit stage involves :

- an explicit predictor, which is identical to the one of the basic Lax-wendroff scheme with matrices, and can be written now :

$$(38)\quad \Delta\tilde{W}_{I,J,K} = -\frac{\Delta t}{2V_{I,J,K}} \int_{\partial\Omega_{I,J,K}} H[W^n, \vec{s}(t), \vec{n}, t] \,|_{t=t^n}\, d\Gamma,$$

- an explicit "S_β^α" numerical flux for the corrector :

$$(39)\quad H_{I,J,K}^{n+1/2} = \int_{\Gamma_{I,J,K}} H[W^n+\Delta\tilde{W}, \vec{s}(t), \vec{n}, t]|_{t=t^{n-1/2}}\, d\Gamma,$$

and finally we get the full explicit approximation :

$$(40)\quad \Delta W_{i,j,k}^{exp} = -\Delta t \frac{\sum_{I,J,K} H_{I,J,K}^{n+1/2}}{V_{i,j,k}}.$$

This scheme does not work without artificial viscosity, but stays second-order time accurate without additional terms.

We have used a simple explicit quasi-TVD correction analogous to the one introduced in [27] and developed for application to the "S_β^α" schemes in the work [28]. This second order correction, in conservation form, is needed in order to smooth the oscillations in the numerical shock structure, and added to the explicit stage (40) under the form :

$$(41)\quad \Delta W_{i,j,k}^{exp} = -\Delta t \frac{\sum_{I,J,K} H_{I,J,K}^{n+1/2}}{V_{i,j,k}} + \sum_{I,J,K} TVD_{I,J,K}^n$$

3.3.3 - Implicit stage for both steady and unsteady problems

The basic implicit stage of the method authorizes the use of high values of the CFL number, and in the context of the solution of steady problems, this allow to increase the intrinsic dissipation of the scheme which depends on the time step. We can obtain steady numerical shock structure without oscillations and without adding dissipation correction. Morever, the speed of convergence to the steady state increases with the CFL number. For unsteady applications, the use of high values of CFL number is still more important for reducing the computational cost.

The implicit stage is a second-order correction in the time-discretization of the Lax-Wendroff scheme introduced in (33):

$$(42)\quad -\frac{\Delta t}{2V_{I,J,K}} \int_{\partial\Omega_{I,J,K}} H(W^{n+1}, \vec{s}, \vec{n})\, d\Gamma.$$

A linearly implicit approximation can be obtained from a time expansion:

$$(43)\quad H(W^{n+1}, \vec{s}, \vec{n}) = H(W^n, \vec{s}, \vec{n}) + A(W^n, \vec{s}, \vec{n})\, \Delta W.$$

We introduce the correction (42,43) in the expression of the explicit corrector (33), corresponding to the linearly implicit part of the numerical flux (35) (see reference [29]) :

$$(44)\quad H_{imp}\,(W^n,\,\Delta W)_{I,J,K} = \int_{\Gamma_{I,J,K}} A(W^n,\,\vec{s},\,\vec{n}\,)\,\overset{o}{\Delta W}\,d\Gamma,$$

where, similarly to the case of the explicit predictor, the expression $\overset{o}{\Delta W}_{I,J,K}$ will depend on each side of the grid-cell $\Omega_{i,j,k}$, and is evaluated in a staggered cell $\Omega_{I,J,K}$ with :

$$(45)\quad \overset{o}{\Delta W}_{I,J,K} = -\frac{\Delta t}{2V_{I,J,K}} \int_{\partial\Omega_{I,J,K}} A(W^n,\,\vec{s},\,\vec{n}]\,d\Gamma.$$

The correction $A(W^n, \vec{s}, \vec{n})\,\Delta W$ introduced in the second-order term is of order Δt. Then, this correction is of the order of the global truncation error of the method and does not reduce its global accuracy in time.

The implementation of the method will be done following two successive stages at each time step :

- an explicit stage leading to the calculation of the explicit corrector (37)
- an implicit stage needing the algebraic solution of the linear problem :

$$(46a)\quad \Delta W_{i,j,k} + \frac{\Delta t}{V_{i,j,k}} \sum_{I,J,K} H_{imp}(W^n,\,\Delta W)_{I,J,K} = \Delta W^{exp}_{i,j,k}$$

$$(46b)\quad W^{n+1}_{i,j,k} = W^n_{i,j,k} + \Delta W_{i,j,k}$$

The direct solution of the fully implicit operator (44),(45),(46) is a difficult problem for which fundamental research is in progress [30]. In order to simplify the problem, the implicit stage (46a) is factorized in each space direction using the "ADI" method. This leads to the solution of triadiagonal linear systems with blocs of size (5x5). An additional simplication consists in replacing the bloc jacobian matrices by their spectral radii leading to, the well known "residual smoothing technique" introduced initially in the work [23]. This simplication allows to reduce notably the number of algebraic operations and the main memory of the computer. In all the cases, the tridiagonal linear systems are solved efficiently using the LU factorization. However, it is well known and proved [19] that the "spectral radius" technique reduces the convergence speed to the steady-state but is compatible with the S^{α}_{β} explicit stage.

3.3.4 - Intrinsic dissipation of the method versus the time-step

We have used, for the steady flow applications, the local time-step technique $\Delta t = \Delta t_{i,j,k}$ in order to maintain a constant value of the CFL number and accordingly a uniform dissipation in the whole computational domain. The intrinsic dissipation of the method is usually sufficient to avoid an additional dissipation correction.

For unsteady flow applications, the time step has to be taken uniform in order to preserve the time consistency and accuracy : $\Delta t = \underset{i,j,k}{\text{Min}}\ \Delta t_{i,j,k}$. Then the value of the CFL number varies in the computational domain. Even in the case of the basic method (Lax-Wendroff explicit stage with matrices), there is not enough intrinsic dissipation to reduce the spurious oscillations in unsteady numerical shock structure. In all the cases, a dissipation correction is necessary to handle unsteady situation.

3.4 - Conservative treatement of the slip condition

We describe in this section a particular boundary condition when the conservative unknowns are evaluated at the solid body surface, submitted to a slip condition $(\vec{V} - \vec{s})\,.\,\vec{n} = 0$. An accurate calculation of the pressure at the wall is possible within a consistent finite volume approximation of the steady momentum conservation equation of (28) written in each cell Ω of the computational domain:

(47) $\int_{\partial\Omega} \vec{H}(W, \vec{s}, \vec{n})\, d\Gamma = \int_{\Omega} \vec{T}(W)\, d\Omega.$

where $\vec{H}$ (resp. $\vec{T}$) is the contribution of the Euler flux (resp. the source term) in the momentum equation of (28) and since the Euler flux has, at a common side Γ_w to the wall, the simple expression (5) :

(48) $\int_{\Gamma_w} \vec{H}(W, \vec{s}, \vec{n})\, d\Gamma = \int_{\Gamma_w} p\, \vec{n}\, d\Gamma$.

Consider now the staggered cell $\Omega_{i,j,3/2}$ of boundary (figure 3):

(49) $\partial\Omega_{i,j,3/2} = \Gamma_{i,j,1} \cup_{I,J,K \neq i,j,1} \Gamma_{I,J,K}$,

such that $\Gamma_{i,j,1}$ is the common side to the solid wall. We describe the momentum conservation (47) in this particular cell and we introduce first the Euler flux contribution at time t^n corresponding to the boundary $\partial\Omega_{i,j,3/2}$ in (49):

(50) $\int_{\partial\Omega_{i,j,3/2}} \vec{H}(W^n, \vec{s}, \vec{n})\, d\Gamma = \int_{\Gamma_{i,j,1}} \vec{H}(W^n, \vec{s}, \vec{n})\, d\Gamma + \sum_{I,J,K \neq i,j,1} \int_{\Gamma_{I,J,K}} \vec{H}(W^n, \vec{s}, \vec{n})\, d\Gamma$.

In the framework of the finite-volume formulation we have the following approximation of the flux at the wall (48) :

(51) $\int_{\Gamma_{i,j,1}} \vec{H}(W^n, \vec{s}, \vec{n})\, d\Gamma = \int_{\Gamma_{i,j,1}} p^n\, \vec{n}\, d\Gamma = p^n_{i,j,1}\, \vec{n}_{i,j,1}$ where $\vec{n}_{i,j,1} = \int_{\Gamma_{i,j,1}} \vec{n}\, d\Gamma$.

the expressions (50), (51) leading to the discrete formulation of (47) :

(52) $p^n_{i,j,1}\, \vec{n}_{i,j,1} = \int_{\Omega_{i,j,3/2}} \vec{T}(W^n)\, d\Omega - \sum_{I,J,K \neq i,j,1} \int_{\Gamma_{I,J,K}} \vec{H}(W^n, \vec{s}, \vec{n})\, d\Gamma$.

The right-hand-side of equation (52) is evaluated in the predictor stage (33) of the current staggered cell $\Omega_{i,j,3/2}$ and we introduce the implicit equation for the pressure :

(53) $p^{n+1}_{i,j,1}\, \vec{n}_{i,j,1} = \int_{\Omega_{i,j,3/2}} \vec{T}(W^n)\, d\Omega - \sum_{I,J,K \neq i,j,1} \int_{\Gamma_{I,J,K}} \vec{H}(W^n, \vec{s}, \vec{n})\, d\Gamma$,

which is now first order time-accurate within a strictly conservative treatement of the steady momentum equation and without any extrapolation for the pressure.

An extention of this treatment is possible when considering a time discretization and a consistent finite-volume approximation of the unsteady Euler equations (28) in the staggered cell with a common side to the solid wall previously describe. With additional help of the mass conservation, we write in a similar way a first order time accurate expression for the pressure at the solid body surface.

4. - NUMERICAL APPLICATIONS

4.1. - Steady flow around multibladed model rotors in hovering-flight

4.1.1 - Introduction

The "absolute" formulation of the Euler equations in the relative frame, described in paragraph 2.3, is used for the application of the method to the hovering-flight problem. It has been chosen instead of the "relative" pseudo-unsteady formulation used in a previous work [16], which is formally exact but leads to a numerical treatment of the finite-volume fluxes less accurate by the fact that the unknowns of the problem depend on the metric through the relative velocity. The treatment of the boundary conditions in the far-field is also improved, with respect to the previous work, by taking into account the information given by the theory of characteristics. The slip boundary condition on the blade surface is applied from the pure conservative treatment, developed in paragraph 3.4, and already used in [16].

4.1.2 - Two-bladed model rotor of US-Army in transonic regime

The implicit Euler method is first applied to the calculation of the steady flow around the two-bladed model of US-Army [31] in hovering flight, for a flow configuration with transonic regime at the blade tip. This classical hovering-flight test-case was calculated in the framework of the Brite/Euram DACRO program [32].

The model rotor has two rectangular, untwisted and untapered blades with constant NACA0012 sections. The aspect ratio Λ of the blades is equal to 6 and the collectif pitch θ_c is equal to 8°. The flow conditions are determinated by the Mach number at the tip of the blade, which value is $M_t = 0.794$.

The construction of the grid is given in details in [16]. We recall that the "C-H" rectangular grid topology needs to model the blade near the hub in order to apply the periodicity boundary condition.

A converged steady Euler solution is obtained with a CFL number equal to 12. Making use of the periodic feature of the flow, the solution on the whole rotor disk surface is represented on figure 4. The comparison with the experiment of US-Army for the pressure distribution around blade sections is rather good (figure 5). However, probably due to the fact that no viscous effects are taken into account in the Euler model, the position of shock waves is slightly pushed farther downstream than in the experiment. No artificial viscosity is added to the method and it is worth pointing out that the numerical shock structure does not exhibit ocillations.

4.1.3. - Fourth-bladed model rotor of IMF of Marseille in hovering-flight

In this case, the method is applied, to the simulation of the steady flow around the fourth-bladed model rotor of IMF of Marseille [33] in hovering-flight. The blades, of aspect ratio $\Lambda = 15$, are rectangular with OA209 airfoil sections, and linearly twisted with a negative slope equal to -8.3. The collective pitch angle θ_c and the conicity angle β of the rotor are respectively equal to 10° and 3° (see figure 6).

In this problem, the computational domain can be restricted to a quarter of a cylinder around one blade by the application of a periodicity boundary condition.

An algebraic grid-generator has been developed in order to also use a "C-H" grid topology in the case of a rotor with more than two blades. The grid is built by projecting two-dimensional "C" grids on cylinders. In order to apply the periodicity boundary condition, these "C" grids are limited by rectangular contours. The complete grid, the construction of which is illustrated on figure 7, is constitued of 140 x 61 x 36 = 307 440 cells. The use of this kind of topology does not need to model the blade near the hub, as it was done in the previous application, but introduces the problem of defining a boundary condition on the arbitrary cylindrical mesh-surface near the center of rotation. A kind of entry or exit subsonic flow condition is applied, at the present time, by testing the orientation of the flow velocity in a direction normal to this surface.

A flow configuration has been calculated in the case of a peripherical rotating velocity corresponding to a Mach number at the tip of the blade of $M_t = 0.315$. A fully subsonic flow is generated around the rotor in these conditions. A converged steady Euler solution, for a mean value of the residual on the density less than 3.10^{-5}, is obtained with a CFL number equal to 10, after 2725 iterations and 2 hours 43 mn on a CRAY YMP computer.

The iso-Mach lines on the blade surface are represented on figure 8. A maximum for the Mach number of the relative flow velocity is reached at the tip of the upper surface of the blade (M = 0.54). A comparison is proposed on figure 9, between the present Euler solution and the experiment of IMFM [33], for the circulation and for the lift coefficient around the blade. It is observed that the position and the intensity of the circulation peak at the tip of the blade are in good agreement with the experiment. This result is very important and shows clearly the interest of an Euler "capture" approach for the hovering-flight problem. The

agreement with the experiment is not so good towards the hub and further investigations have to be achieved to complete the assessment of this Euler hover code.

4.2. - Unsteady flow around rotor blades in forward-flight

4.2.1 - Isolated blade in non-lifting case

As a first unsteady application, the simulation of the flow around an isolated blade in forward flight without pitching and flapping motions is considered. The blade, of aspect ratio $\Lambda = 7$, is rectangular, untwisted and untapered with NACA0012 airfoil sections. A non-lifting flow configuration is derived by equalling the incidence of the blade to zero. The rotating velocity ω is defined by the value of the Mach number at the tip of the blade noted $M_{\omega R} = \omega R/a_0 = 0.80$, where R is the blade radius and a_0 is the speed of sound in the unperturbed flow. The advance ratio $\mu = 0.20$ corresponds to a Mach number in the unperturbed flow equal to $M_0 = \mu.M_{\omega R} = 0.16$.

This problem was previously introduced in the work [34] for the validation of a new unsteady Euler method. Experimental results are also available [36]. The formulation described in paragraph 2.2.3, and the numerical method developed for unsteady time-accurate applications (see paragraph 3.3.2), are used to solve this problem.

The computational grid has a topology similar than the one previously used for the problem of the two-bladed NACA0012 model rotor in hovering-flight. It is composed of 140 x 27 x 41 = 154980 cells with 25 C-grids distributed along the blade.

The unsteady Euler calculation is initiated, as it is done in the work [34], from a quasi-steady solution obtained for a fixed value of the azimuthal angle. For stability constraints, a maximum value of the local CFL number, reached in the smaller cell near the leading edge of the blade, was chosen equal to 10. A cycle of the unsteady evolution is described with 3600 time-steps for this value of the CFL number. The periodic regime is obtained after about two unsteady cycles leading to a global CPU cost (taking into account the preliminar quasi-steady calculation) of 2 hours and 24 minutes on a CRAY YMP computer. The unsteady Euler code consumes 7.7 microseconds of CPU time per time-step and per grid-cell.

The periodic solution is described on figures 10 and 11. The variation of the local pressure coefficient around a section located at the tip of the advancing blade (r/R = 0.90), is plotted for several values of the azimuthal angle on figure 10. Due to the addition of a quasi-TVD correction, the numerical moving shock structure is not oscillating. A good agreement of the calculated pressure distributions with the experiment [35] can be observed. Finally, the iso-Mach lines for the relative Mach number, represented on figure 11, show that the numerical solution is regular, on the blade surface, near the hub and in the far-field.

4.2.2 - Three-bladed ONERA model rotor in forward-flight with cyclic pitching and flapping motions

The method is then applied to the simulation of the unsteady flow around the ONERA three-bladed model rotor in forward flight with cyclic pitching and flapping motions. The blades have a rectangular shape with "PF1" parabolic tip. The rotor shaft angle is equal to $-12.4°$ and the advance and motion conditions are the following :

$$M_{\omega R} = 0.613$$

$$\mu = 0.40$$

$$\theta(t)° = 14.16 + 0.43\ \cos\psi(t) - 5.14\ \sin\psi(t)$$

$$\beta(t)° = 01.25 - 5.12\ \cos\psi(t) + 0.32\ \sin\psi(t)$$

For the solution of this more realistic problem, an isolated blade Euler calculation is made by the formulation described in paragraph (2.2). The exact solid body motion of the blade is taken into account in this approach.

The influence of the other blades is simulated, in an approximate way, by introducing,

during the unsteady process, a wake correction supplied by the lifting-line incompressible code METAR [36]. This kind of wake correction is a classical one, and was previously introduced at ONERA in the framework of the development of potential codes [37]. The METAR code gives the velocities induced by the wake. We can deduce, from these velocities, some induced incidences α_i [r, ψ(t)], depending on the blade radial position r and on the azimuthal angle ψ(t). The wake correction consists in adding a local pitching motion to the blade surface with an angle α_i. This is simply realized by rotating, with an angle α_i, the local normal $\vec{n}$ to the blade, while applying the slip boundary condition on the blade surface.

A partial view of the grid, composed of 138x25x40= 138 000 cells, is shown on figure 12. The extension of the grid is about one blade radius length in all the directions.

The maximum of the local CFL number used in the calculation is equal to 10, and the computing time needed for describing one cycle of the unsteady evolution is equal to about one hour on a CRAY YMP computer.

The variation of the induced incidences versus the azimuthal angle and for some blade sections near the blade tip, is shown on figure 13. It is observed that the wake influence is all the more important as one is near the blade tip in the advancing blade, with a maximum for the azimuth $\psi = 30°$.

The variation of the lift coefficient around the section r/R = 0.90 is plotted on figure 14 for an isolated-blade Euler simulation, an Euler multibladed simulation with wake correction, and for the ONERA experiment. It is observed, as noticed before, that the wake correction operates mainly in the advancing blade. The discrepency between the Euler calculations and the experiment, at azimuth $\psi = 0$, is probably due to the presence of the shaft rotor which is not taken into account in the calculations. However, a rather good agreement between the two calculations and the experiment is obtained. The good agreement, between the Euler multibladed simulation and the experiment, is confirmed for the distribution of the pressure coefficient around the blade section considered (see figure 15). The iso-Mach lines for the relative Mach number at four azimuthal blade positions are described on figure 16. One can observed the evolution of the transonic pocket near the leading edge at the tip of the blade. As in the previous application, the flow solution is smooth in the whole computational domain.

5. - CONCLUSION

An original implicit-space centered Euler method has been developed for the numerical simulation of steady and unsteady flows around multibladed helicopter rotors. It has been possible to calculate the flow around rotors in hovering-flight without adding any dissipation correction, even in the transonic regime, because of the sufficient intrinsic dissipation of this method, when applied to the solution of a steady problem. For the application to transonic unsteady forward-flight problems, the dissipative properties of the method have been strengthened by the addition of a simple quasi-TVD correction which maintains the second-order time-accuracy.

The use of a formulation for the absolute velocity in the relative frame has improved the results previously obtained for the simulation of the flow around the two-bladed model rotor of US-Army.

An algebraic grid-generator, well-suited for the construction of cylindrical grids with "C-H" topology, has been developed for the application to a rotor with more than two blades.

The application of the method to the fourth-bladed model rotor of IMFM, in the framework of a pure capture of the wake, has shown the ability of an Euler approach to represent some of the major features of the hovering-flight problem.

The method has been extended to the unsteady situation in order to calculate the flow

around an isolated blade in forward-flight with arbitrary solid body motion.

The introduction of a wake correction, for taking into account of the mutual influence of blades, has allowed a promising comparison with the experiment in the case of the ONERA three-bladed model rotor with cyclic pitching and flapping motions.

Further work will be achieved for a capture of the unsteady wake system in the framework of a multidomain Euler calculation for the whole rotor.

REFERENCES

[1] Roberts W. and Murman E.M. - Solution method for a hovering helicopter rotor using the Euler equations. AIAA Paper 85-0436.

[2] Sankar N.L., Wake B.E. and Lekoudis S.G. - Solution of the unsteady Euler equations for fixed and rotor wing configurations. J. Aircraft, vol. 23, no 4, April 1986, p. 283-289. Also AIAA Paper 85-0120.

[3] Roberts W. and Murman E.M. - Euler solutions of the flow around a hovering helicopter rotor. AIAA Paper 86-1784.

[4] Agarwall R.K. and Deese J.E. - Euler calculations for flowfield of a helicopter rotor in hover. J. Aircraft, vol. 24, no 24, April 1987, p.231-238. Also AIAA Paper 86-1782.

[5] Agarwall R.K. and Deese J.E. - An Euler solver for calculating the flowfield of a helicopter rotor in hover and forward flight. AIAA Paper 87-1427.

[6] Chang I.C. and Tung C. - Euler solution of the transonic flow for a helicopter rotor. AIAA Paper 87-0523.

[7] Chen C.L., McCroskey W.J. and Ying S.X. - Euler solution of a multiblade rotor flow. Vertica, Vol. 12, Oct. 1988, pp. 303-313, presented at the 13th European Rotorcraft Forum, Arles, France, (1987).

[8] Chen, C.L. and McCroskey, W. J. - Numerical simulation of helicopter multi-bladed rotor flow. AIAA Paper 88-0046, janv. 1988.

[9] Strawn R. C. and Barth T. J. - A Finite-volume Euler solver for computing rotary-wing aerodynamics on unstructured meshes. Proceedings of 48th Annual Forum of the AHS, Washington, June 3-5, 1992.

[10] McCroskey W.J - Some recent applications of Navier-Stokes codes to rotorcraft. Fifth Symposium on numerical and physical aspect of aerodynamic flows, Long Beach, CA, Jan. 13-16, 1992.

[11] Kroll N. - Computation of the flow fields of propellers and hovering rotors using Euler equations. 12th European Rotorcraft Forum, Paper no 28, Garmish-Partenkirchen, Germany, Sept. 1986.

[12] Stahl H. - Application of a 3D Euler code to transonic blade tip flow. 12th European Rotorcraft Forum, Paper no 29, Garmish-Partenkirchen, Germany, Sept. 1986.

[13] Kramer E., Hertel J. and Wagner S. - Computation of subsonic and transonic helicopter rotor flow using Euler equations. Vertica, Vol. 12, No. 3, 1988, presented at the 13th European Rotorcraft Forum, Paper no 2-14, Arles, France, Sept. 1987.

[14] Kramer E., Hertel J. and Wagner S. - A study of the influence of a helicopter rotor blade on the following blades using Euler equations. 14th European Rotorcraft Forum. Paper no 2-6, Milano, Italy, 1988.

[15] Kramer., Hertel J. and Wagner S. - Euler procedure for calculation of the steady rotor flow with emphasis on wake evolution. AIAA Paper 90-3007.

[16] Sidès J. and Boniface J.C. - Solution of the compressible Euler equations for steady flows around helicopter rotor blades by an implicit space-centered method. Proceeedings of 17th European Rotorcraft Forum, Paper no 91-40, Berlin, September 23-27, 1991. Also TP

ONERA no 1991-177.

[17] Lerat A. and Sidès J. - Numerical simulation of unsteady transonic flows using the Euler equations in integral form. Israel J. Tech., vol. 17, p 302-310, 1979.

[18] Lerat A. - Sur le calcul des solutions faibles des systèmes hyperboliques de lois de conservation à l'aide de schémas aux différences. ONERA Publication 1981-1.

[19] Lerat A. - Implicit methods of second-order accuracy for the Euler equations. AIAA Paper 83-1925. Also AIAA J. 23, 33-40, 1985.

[20] Daru V. and Lerat A. - An implicit centered scheme which gives non-oscillatory steady shocks. International Conference on hyperbolic problems, Saint-Etienne, France, jan. 13-17, 1986.

[21] Lerat A. and Sidès J. - Efficient solution of the steady Euler equations with a centered implicit method. In : Num. Meth. Fluid Dyn. III, RK.W. Morton and M.J. Baines Eds., Clarendon Press, Oxford, p.65-86, 1988. Also TP ONERA 1988-128.

[22] Lerat A. and Sidès J. (1989). Implicit transonic calculations without artificial viscosity or upwinding. Proceedings of "GAMM - Workshop on the numerical solution of compressible Euler flows". Notes on Numerical Fluid Mechanics 26, 1989, p. 227-250.

[23] Lerat A., Sidès J. and Daru V. - An implicit finite-volume method for solving the Euler equations. Lecture Notes in Physics, vol. 17, p.343-349, 1982.

[24] Lerat A., Sidès J. and Daru V. - Efficient computation of steady and unsteady transonic flows by an implicit solver. Advances in Computational Transonics. vol. IV, p. 543-575, Ed. Habashi W.G., Pineridge Press, 1985.

[25] Sidès J. - Computation of unsteady transonic flows with an implicit numerical method for solving the Euler equations. La Recherche Aérospatiale no 2, 1985.

[26] Sens A.S. - Calcul d'écoulements transsoniques instationnaires par résolution implicite centrée des équations d'Euler sans viscosité artificielle. ONERA Publication 1990-8, 1990.

[27] Davis S.F. - TVD finite difference schemes and artificial viscosity. NASA CR 172373. ICASE Report no 84-20, 1984.

[28] Jacque-Sabatier F. - Corrections de flux TVD pour les schémas centrés S_β^α et application à l'étude des écoulements compressibles instationnaires dans les canalisations de moteurs. Thesis, Paris 6 University, 1987.

[29] Lerat A. - Difference methods for hyperbolic problems with emphasis on space-centered approximations. ONERA Publication 1990-4, 1990.

[30] Khalfallah K., Lacombe G. and Lerat A. - Analysis of implicit treatments for a centred Euler solver. To appear in Computers and Fluids (1993).

[31] Caradonna F.X. and Tung C. - Experimental and analytical studies of a model helicopter rotor in hover. NASA TM-81232, 1981.

[32] Final DACRO Report, Brite Euram AERO-0005-C(MB)-1109, February 1992.

[33] Favier D., Nsi Mba M., Barbi C. and Maresca C. - A Free wake analysis for hovering rotors and advancing propellers. Vertica, vol. 11, no 3, p. 493-511, 1987.

[34] Chen C.L., McCroskey W.J. and Obayashi S. - Numerical solutions for forward-flight rotor flow using an upwind method. J. Aircraft, vol. 28, no 6, 1991.

[35] Caradonna F.X. Laub, G.H. and Tung C. - An experimental investigation of the parallel blade-vortex interaction. NASA TM-86005, nov. 1984.

[36] Toulmay F. - Modèle d'étude de l'aérodynamique du rotor. Formulation et application au 3496.V., Aérospatiale Report H/D.E.R. 37176.

[37] Costes M., Desopper A., Céroni P. and Lafon P. - Flow field prediction for helicopter rotor with advanced blade tip shapes using CFD techniques. Proceedings of 2nd Int. Conf. on Basic Rotorcraft Research, College Park (University of Maryland), USA, Feb. 1998. Also ONERA TP no 1998-17.

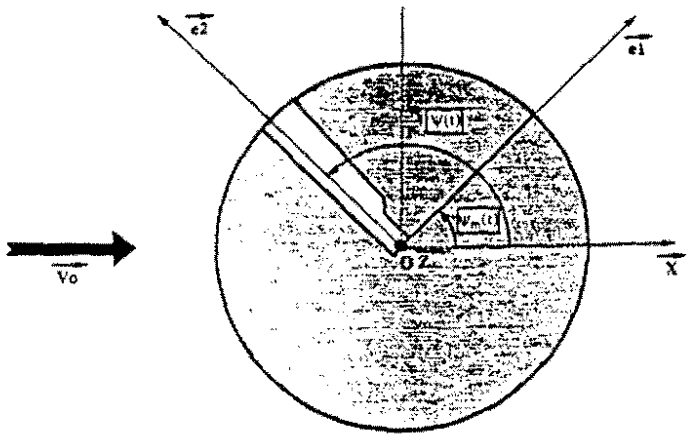

ROTATION MOTION

Figure 1a

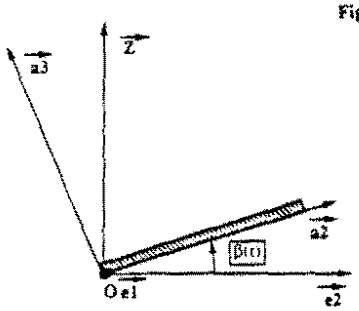

FLAPPING MOTION

Figure 1b

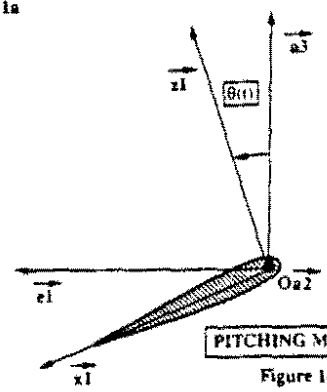

PITCHING MOTION

Figure 1c

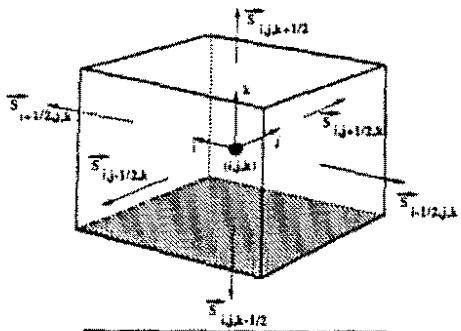

OUTWARD NORMAL TO SURFACES I,J,K

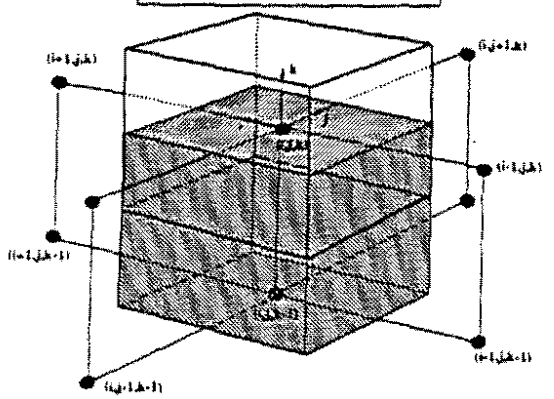

BASIC CORRECTOR CELL AND STAGGERED PREDICTOR CELL

Figure 2

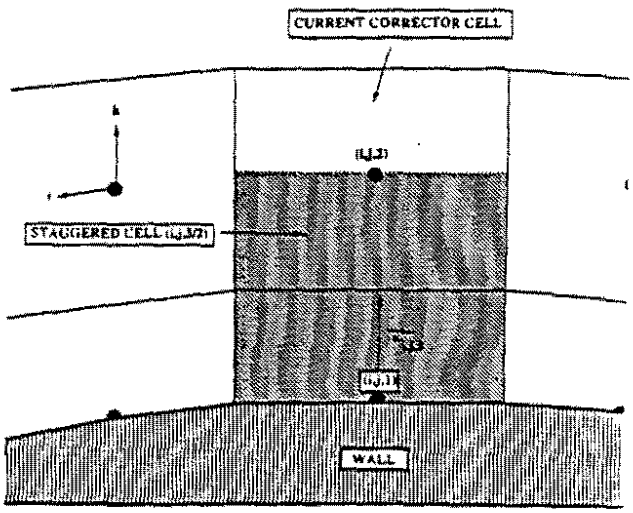

CONSERVATIVE TRAITEMENT OF THE SLIP CONDITION

Figure 3

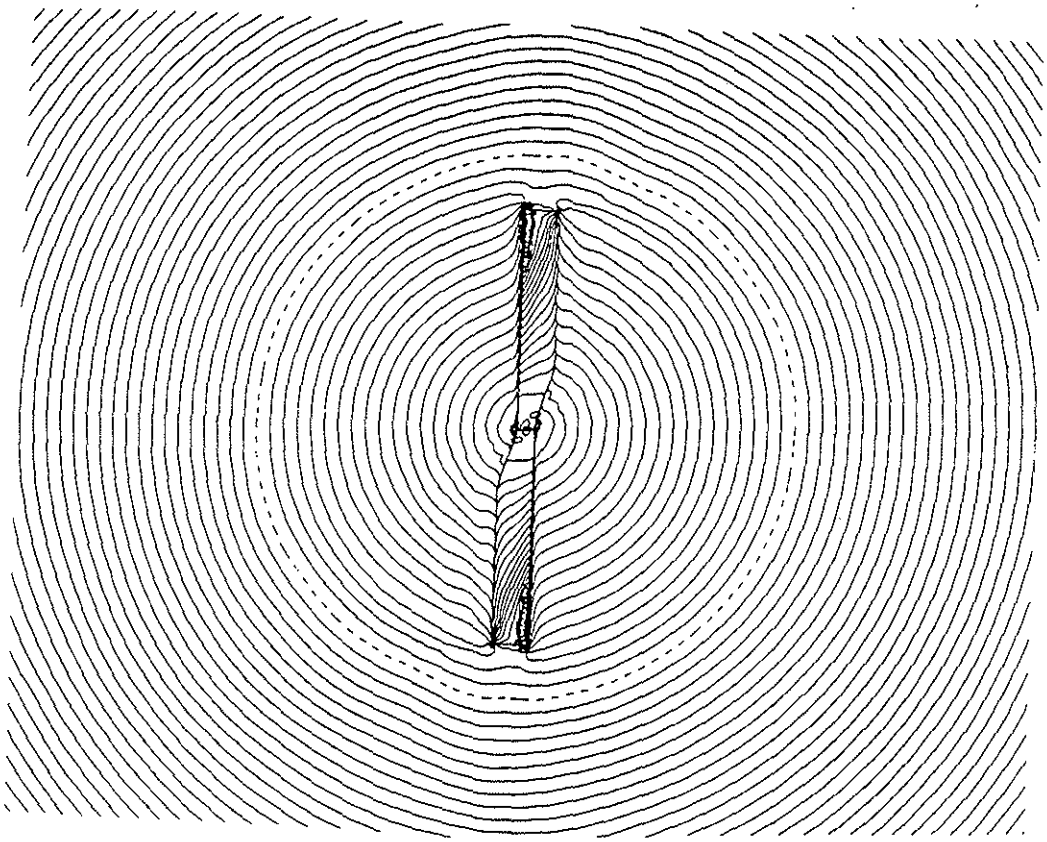

Figure 4 - Iso-Mach lines for relative Mach number ($\Delta M_r = 0.05$)
on the upper surface of the rotor disk

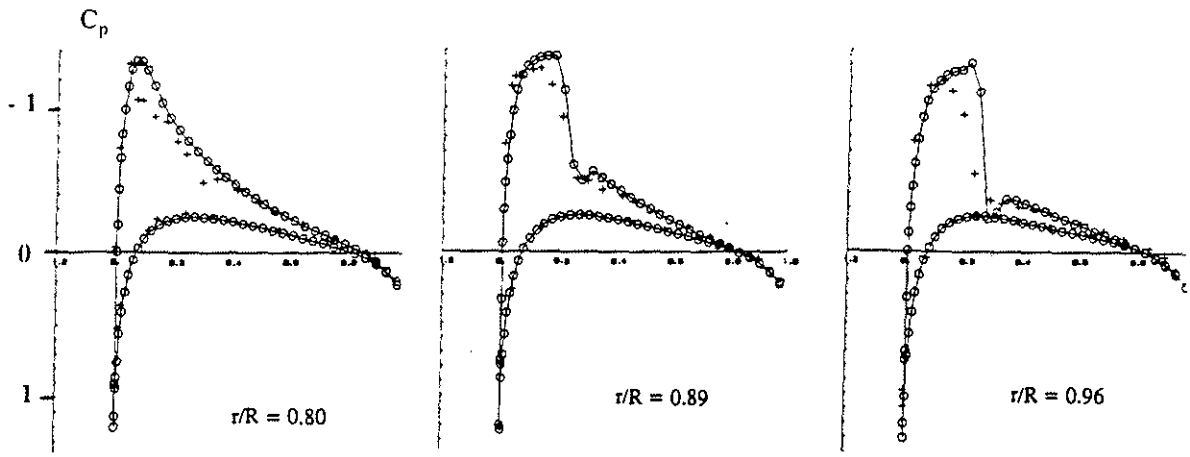

Figure 5 - Pressure coefficient around blade sections
(o o present Euler method, + + experiment [31])

TWO-BLADED NACA0012 MODEL ROTOR OF US-ARMY IN HOVERING-FLIGHT
($M_t = 0.795$, $\theta_c = 8°$, $\Lambda = 6$)

Conicity of rotor : $\beta = 3^o$

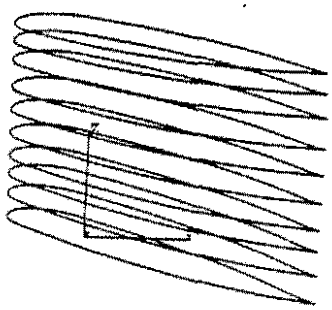

OA209 profile

Collective pitch : $\theta_c = 10^o$

Linear twist : $= -8^o$

Figure 6 - Geometry

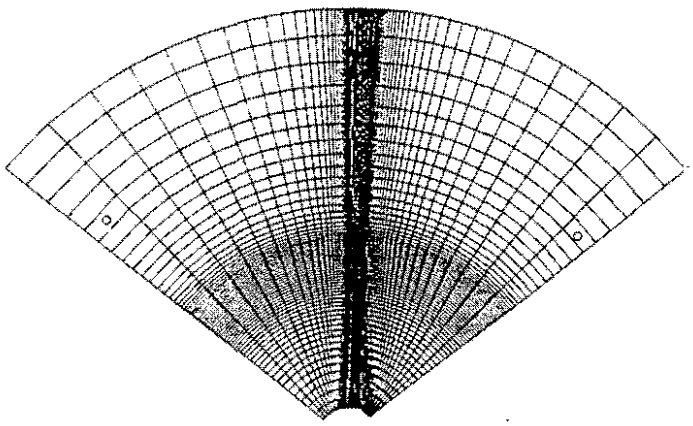

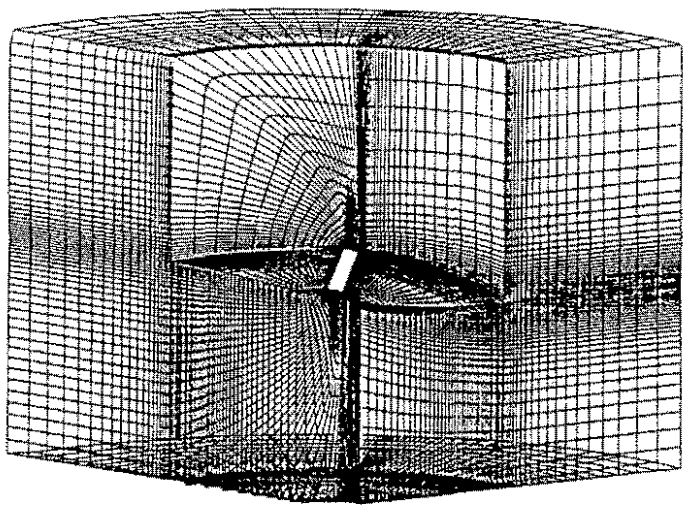

Figure 7 - Partial view of computational grid

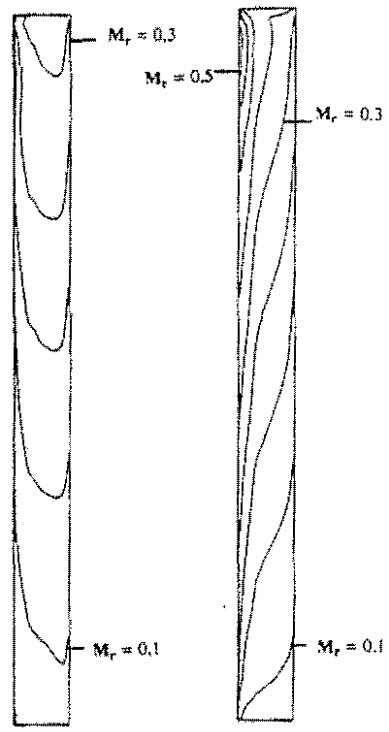

Figure 8 - Iso-Mach lines on the blade surfa

FOUR-BLADED MODEL ROTOR OF IMF OF MARSEILLE IN HOVERING-FLIGHT

($M_t = 0.315$, $\theta_c = 10^o$, $\Lambda = 15$)

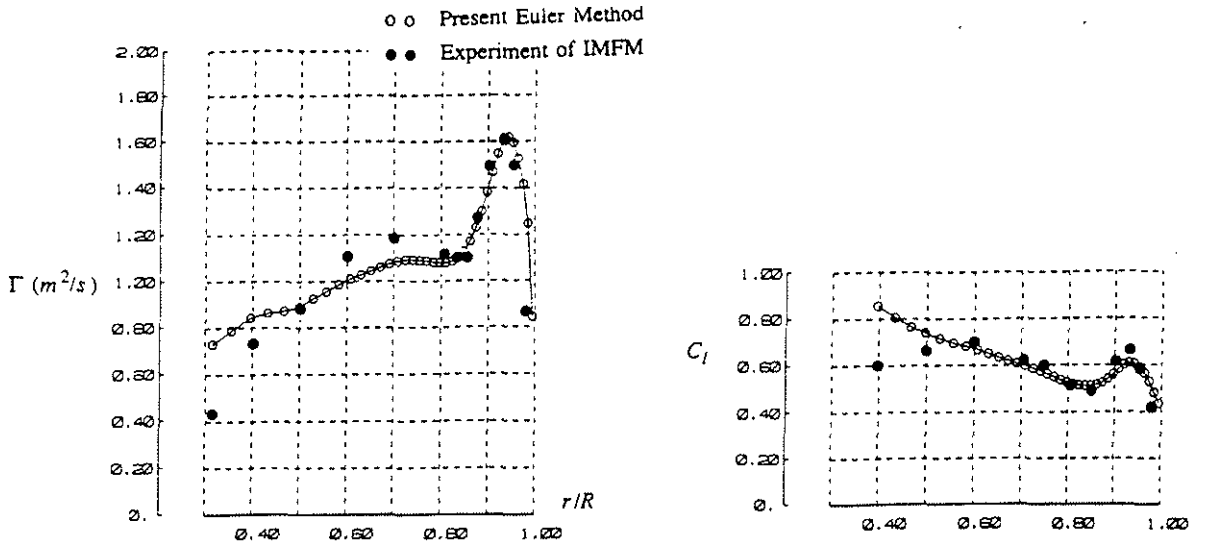

Variation of circulation around blade sections

Variation of lift coefficient around blade sections

Figure 9 - FOUR-BLADED MODEL ROTOR OF IMF OF MARSEILLE IN HOVERING-FLIGHT
($M_t = 0.315$, $\theta_c = 10°$, $\Lambda = 15$)

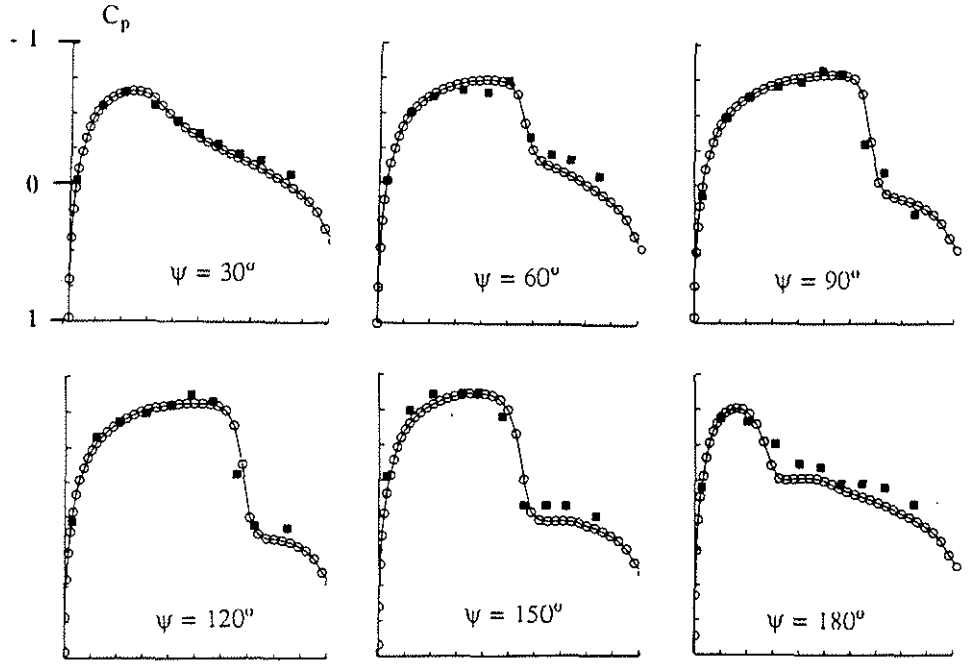

Figure 10 - Variation of unsteady pressure coefficient at the tip of advancing blade (r/R = 0.89)
(o o present Euler method, + + experiment [35])

ISOLATED NACA0012 ROTOR BLADE IN FORWARD-FLIGHT

($\alpha = 0°$, $M_{\Omega R} = 0.8$, $\mu = 0.2$)

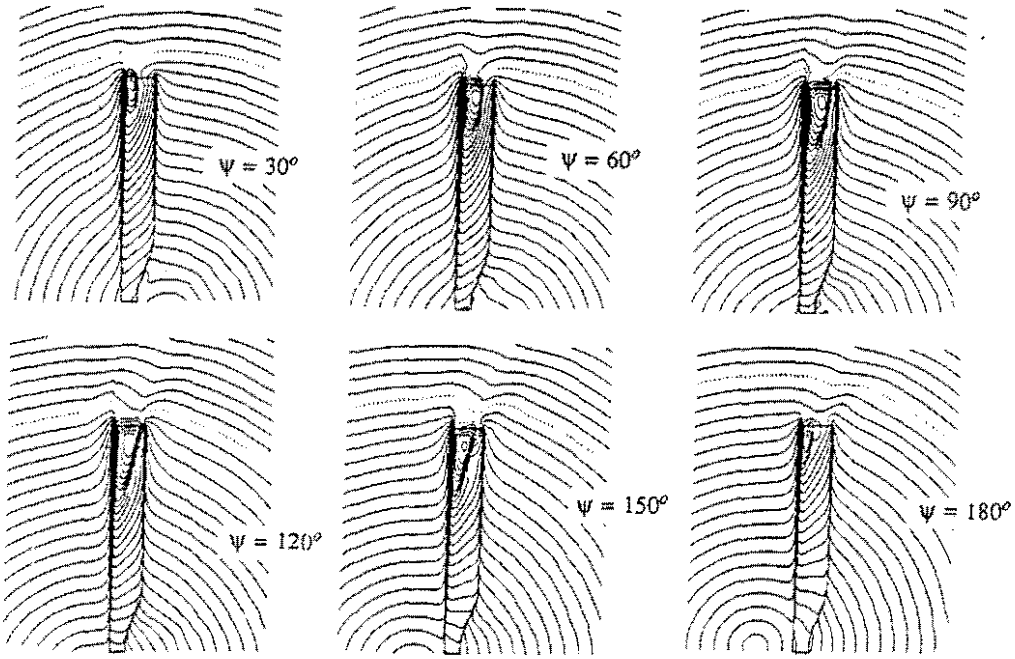

Figure 11 - Iso-Mach lines for relative Mach number ($\Delta M_r = 0.05$)

ISOLATED NACA0012 ROTOR BLADE IN FORWARD-FLIGHT

($\alpha = 0°$, $M_{\Omega R} = 0.8$, $\mu = 0.2$)

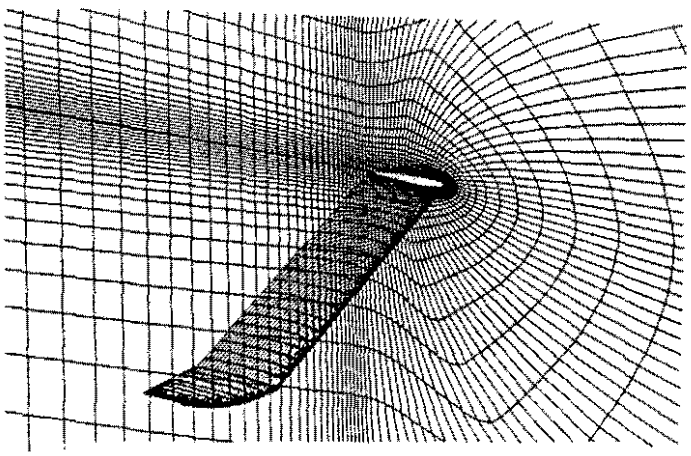

Figure 12 - Partial view of the grid

$M_{\Omega R} = 0.613$

$\mu = 0.40$

$\theta(t)° = 14.16 + 0.43 \cos\psi(t) - 5.14 \sin\psi(t)$

$\beta(t)° = 01.25 - 5.12 \cos\psi(t) + 0.32 \sin\psi(t)$

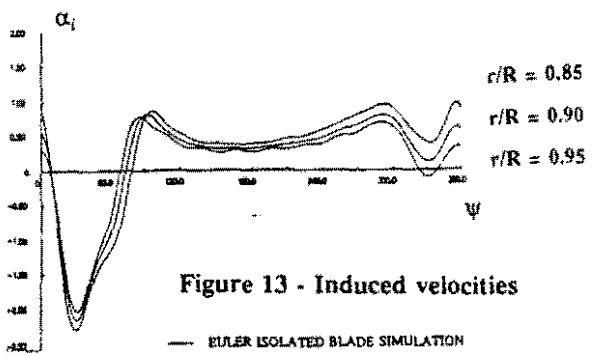

Figure 13 - Induced velocities

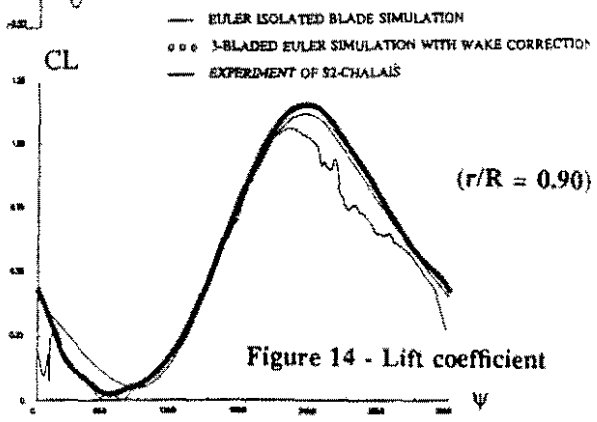

Figure 14 - Lift coefficient

THREE-BLADED ONERA MODEL ROTOR with PF1 Blades IN FORWARD-FLIGHT motion with CYCLIC PITCH and FLAPPING

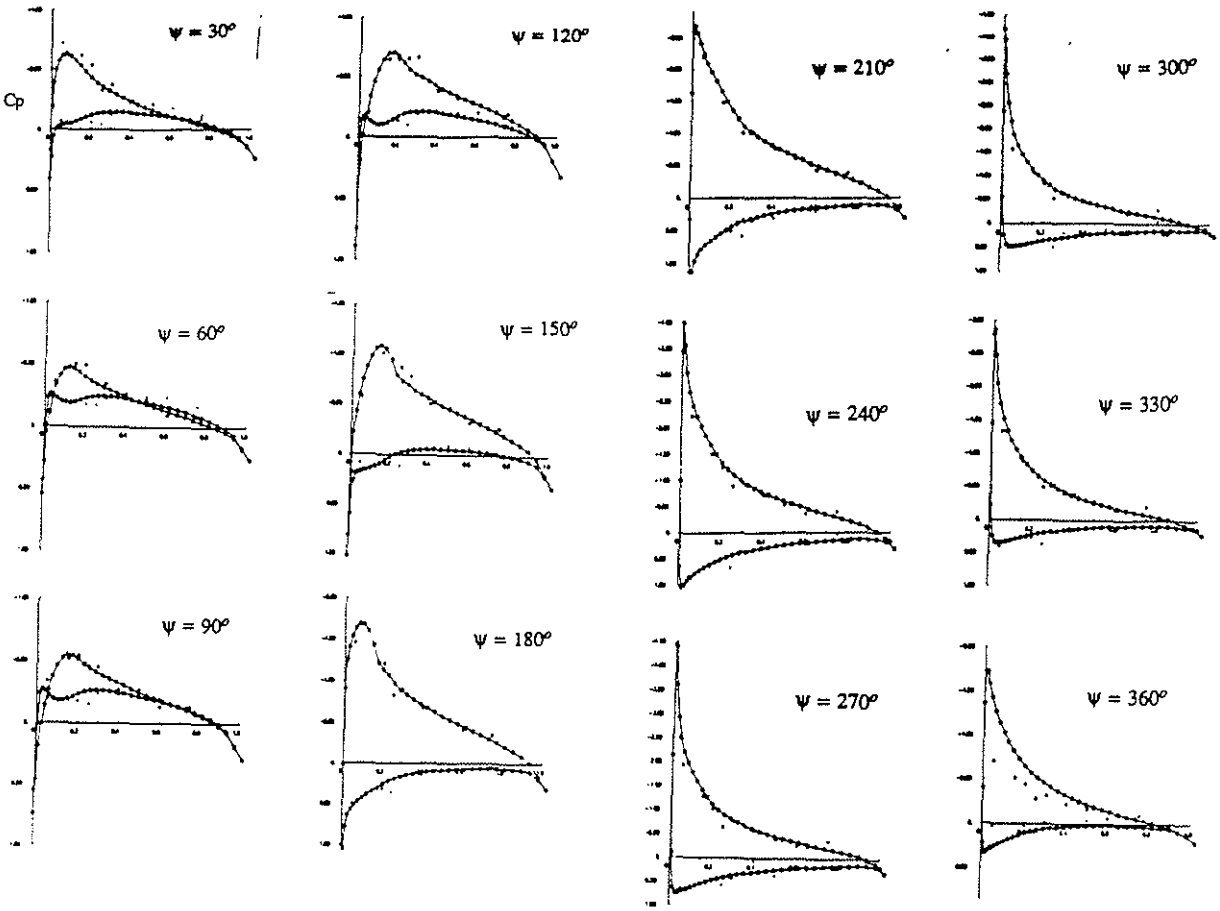

Figure 15 - Variation of unsteady pressure coefficient around blade section (r/R = 0.90).
o Euler calculation with wake correction,
* upper surface, + lower surface : experiment of S2-Chalais.

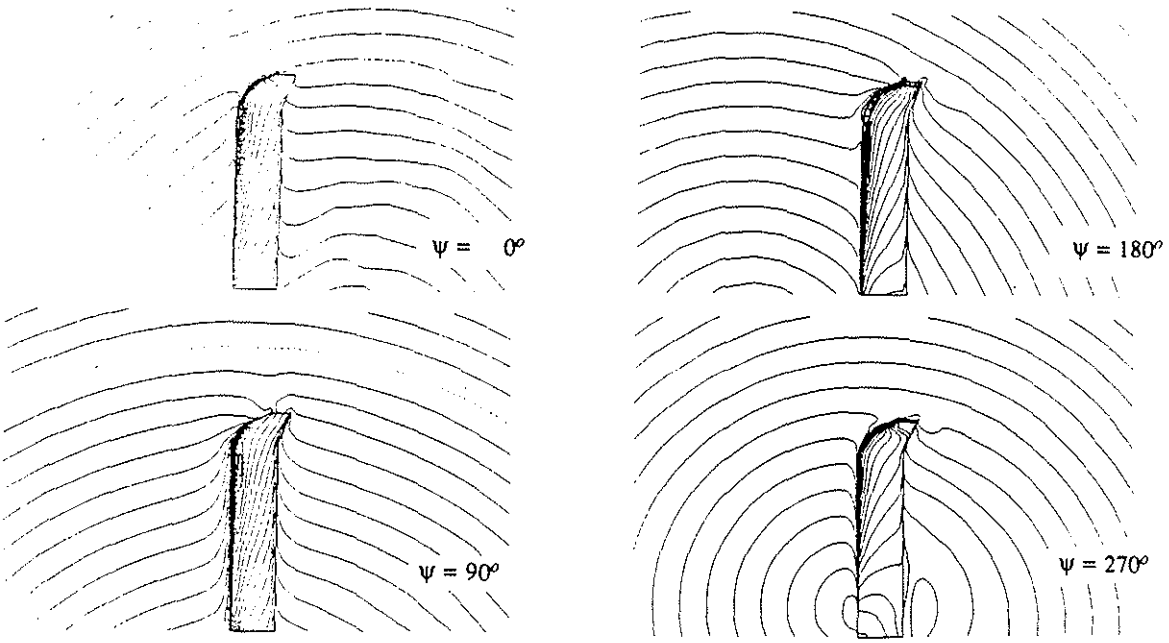

Figure 16 - Isomach-lines on the blade upper-surface